Optical biopsy of laryngeal lesions using femtosecond multiphoton microscopy

HONG ZHANG,[1,3] **YAN CHEN,**[2,3] **DINGFANG CAO,**[1] **WENJING LI,**[1] **YANLEI JING,**[1] **HUA ZHONG,**[2] **HONGGANG LIU,**[1,4] **AND XIN ZHU**[2,5]

[1]*Department of Pathology, Beijing Tongren Hospital, Capital Medical University; Beijing Key Laboratory of Head and Neck Molecular Diagnostic Pathology, Beijing 100730, China*
[2]*Femtosecond Research Center (Guangzhou), A616 80 Lanyue Road, Guangzhou 510663, China*
[3]*These authors contributed equally to this work*
[4]*liuhg1125@163.com*
[5]*zhuxin@femtoresearch.com*

Abstract: Laryngeal squamous cell carcinoma (LSCC) is one of the most prevalent malignancy of the upper aerodigestive tract. Detection of early lesions *in vivo* could improve the survival rate significantly. In this study, we demonstrated that femtosecond multiphoton microscopy (MPM) is an effective tool to visualize the microscopic features within fixed laryngeal tissues, without sectioning, staining, or labeling. Accurate detection of lesions and determination of the tumor grading can be achieved, with excellent consistency with conventional histological examination. These results suggest that MPM may represent a powerful tool for in-vivo or fast ex-vivo diagnosis of laryngeal lesions at the point of care.

1.   Introduction

Laryngeal cancer represents a form of malignancy originating from the epithelium or the connective tissue of larynx, which can be divided into supraglottic larynx, the glottis and the subglottic region. It is the most prevalent type of human head and neck tumors in many countries, accounting for 1% to 2.5% of all human neoplasms, with 177,422 new cases and 94,771 deaths in 2018 worldwide [1]. In terms of histopathology, a majority of larynx malignancies (around 95%) are squamous cell carcinoma (LSCC), with chondrosarcomas, leiomyosarcomas and melanomas accounting for the other 2%-5% [2].

The prognosis of laryngeal cancer depends on a number of individual factors, including tumor size and location, depth of invasion, histopathological type, degree of differentiation and presence of metastasis. It was reported that patients with early laryngeal cancer (T1-T2N0) had a 5 year survival rate of higher than 80% [3]. Unfortunately, 50-75% of the patients are diagnosed at advanced stages (stage III or IV) which significantly limited the efficacy of the treatments [2,4]. It's often difficult to detect early laryngeal lesions using conventional laryngoscope with white light imaging. Currently the diagnosis is still solely based on the histopathological assessment on the biopsy specimens, which relies on the accurate sampling followed by tissue sectioning and hematoxylin and eosin (H&E) staining. Sensitive and accurate diagnosis of early laryngeal cancer can be very challenging due to lack of reliable biomarkers and often require special staining or immunostaining to visualize specific structures or cell types. These conventional histological analyses are time-consuming and labor-intensive. It's difficult to generate multiple staining contrasts simultaneously with exact spatial co-registration which could increase the risk of missing small lesions. Therefore, there is a great need for developing fast, sensitive, and accurate methods which enable in vivo and point of care screening and diagnosis for early stage laryngeal cancer.

A variety of label free and slide free imaging techniques, which are usually based on nonlinear optical processes with femtosecond laser pulses, have been developed and widely used for

biological tissue imaging in the past years [5–7]. Autofluorescence (AF) of the tissue, including two-photon and three-photon excitation fluorescence (2PEF and 3PEF), arises when endogenous fluorophores were excited by light at suitable wavelength. The most common endogenous fluorophores include intracellular molecules such as NAD(P)H, FAD, porphyrins, lipo-pigments, as well as extracellular components such as elastin. Many of these biomolecules play key functional roles in a living system. AF allows the direct observation of the cellular morphology and metabolic states without using exogenous labeling agents, ideal for *in vivo* and fresh *ex vivo* tissue imaging. Recently it has been used for intraoperative lesion detection and studying the changes during carcinogenesis, tumor progression, and metastasis [8–10]. Collagen fibers with non-centrosymmetric structure, could produce strong second harmonic generation signals (SHG) [11], providing a unique modality for imaging the fibrous structure in the extracellular matrix and the basement membrane. It has been suggested that the changes in the length, thickness, orientation and alignment of the collagen fibers are sensitive and quantifiable indicators for evaluating response to treatments, tumor aggressiveness and predicting prognosis and the tendency of metastasis [12,13]. Additionally, THG microscopy is an important label free technique that has been used to study a broad range of tumors [14,15]. THG signal generates from inhomogeneous interfaces with changes in refractive index. Therefore, it can be used to image cellular membranes, nuclear membranes, lipid droplets and other intracellular or extracellular structures [16,17].

The combination of AF, SHG and THG integrates the strengths of these techniques and affords a unique and powerful tool for the direct visualization of the tissue structure and cellular morphology. MPM has been successfully applied for the detection of malignant lesions in various type of cancers, including oral [5,18,19], esophageal [20,21], breast [22,23], and colorectal [24,25]. Being label free and slide free, this novel technique could potentially enable *in vivo* optical biopsy for cancer research and diagnosis at the point of care. Therefore, in this study we investigated whether the femtosecond label-free imaging (FLI) microscopy could provide images for accurate histological evaluation of laryngeal tissues without using exogenous labeling agents, which indicates the potential for in vivo detection of the lesions for laryngeal cancer.

2. Materials and methods

2.1. Sample preparation

This study was approved by the ethics committee of Beijing Tongren Hospital of Capital Medical University in Beijing, China. Resected specimens were obtained from the primary tumors and normal regions that were at least 2 cm away from the tumor margins, from 6 patients with Laryngeal squamous cell carcinoma, resulting in 12 samples in total. All the tissue samples were fixed using 10% formalin within 30 min of surgery and stored in 4°C. MPM microscopy imaging was performed on fixed and unsectioned tissue blocks within 48 hours without staining. Immediately after the imaging session, tissue blocks were embedded in paraffin and sectioned into several 5-μm-thick serial sections, followed by different staining techniques including standard H&E staining, Masson's trichrome staining, and Feulgen's staining.

2.2. MPM imaging

All MPM images were acquired using femtosecond label-free imaging (FLI) microscopy system (Femtosecond research center, Guangzhou, China). The experimental setup is illustrated in Fig. 1, inspired by the optical setup reported in [22]. The excitation source is a home-built femtosecond fiber laser with spectra spanning from 900-1200 nm with a 13.6 MHz pulse repetition rate. A typical spectrum from the light source is shown in Fig. 1(a). The laser pulses were guided into a home-built pulse shaper for pulse compression based on the MIIPS method described in Ref. [26] and further wavelength range picking. The autocorrelation trace of the pulse at the sample

position is shown in Fig. 1(b), supporting our observation of sub-40 fs pulse. The beam is then raster scanned by a 2D galvo-scanning system, expanded by a telescope to illuminate the entire back aperture of the objective so that the smallest possible focal spot size can be achieved. An objective with high transmission from UV to near IR and high numerical aperture (UAPON 40XW340, Olympus, NA 1.15) was used to produce a large field of view and highly resolved image. Samples are placed on coverslips with a uniform thickness of $170 \pm 5\,\mu m$ (manufactured with Schott D 263 M glass), and moved by a high-precision automated xyz stage (ASI Imaging, Inc). Back-scattered signals are separated into multiple channels (THG 340-380 nm; 3PEF 415-526 nm; SHG 530-570 nm, etc.) using a non-descanned detection scheme enabled by a set of dichroic mirrors and bandpass filters (Semrock, Inc), focused with 50 mm focal length lenses, and recorded simultaneously by high sensitivity PMTs (H7421-40, Hamamatsu). Images from individual channels can be merged to form a composite image with pseudo colors (THG-yellow; 3PEF-mengenta; SHG- green).
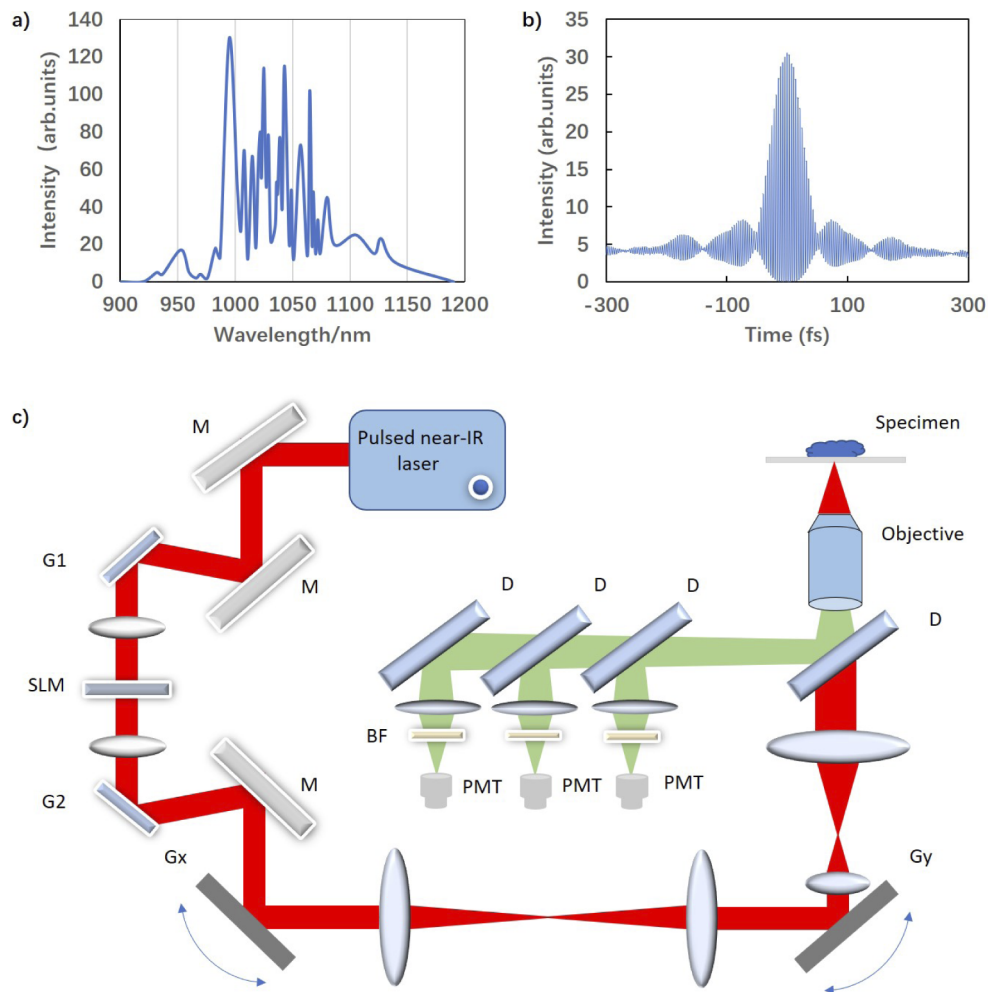

Fig. 1. a) Spectrum from the laser source; b) autocorrelation trace of the pulses at the sample position; c) Schematic of the FLI microscopy system. M: mirrors; D: dichroic mirrors; BF: bandpass filters; Gx & Gy: scanning mirror X & Y; G1 & G2: gratings; SLM: spatial light modulator

Each image was acquired with a field of view 380×380 μm^2, sampled with 500×500 or 1000×1000 pixels in 1 to 4 second. To scan a larger area, serial images were acquired by moving the motorized translational stage, with a 15% overlap to remove any edge artifacts during digital mosaicking. For each patient, at least one normal region and one tumor region were imaged with MPM, and the sizes of stitched images ranged from 6×6 mm up to 10×10 mm.

2.3. Data analysis

Both MPM images and conventional histological slides were evaluated and compared by experienced pathologists. Histological features from the MPM images were identified by comparing to the H&E slide images from similar regions of the same sample. For the analysis of collagen fiber, regions of interest (ROI) including two invasive tumor regions and two normal regions far from the tumor boundary with the size of 1×1 mm were selected from each patient for analysis. The alignment of collagen fibers were performed with Curvealign software [27–29]. Curvealign is an open-source, free MATLAB software to analyze collagen fiber by directly finding optimal representation of fiber edges using the curvelet transform. This framework allows the measurement of fiber alignment on a global, region of interest, or fiber basis, as well as the fiber angle relative to a defined boundary. In current study, "alignment coefficient" ranging from 0-1 is calculated which measures the alignment of fibers with respect to each other, with higher value indicating more aligned fibers. The statistical difference in the fiber alignment between normal and malignant regions were analyzed by paired t-test using IBM SPSS Statistics 24 software.

3. Results

MPM microscopy images demonstrate sufficient resolution and contrast to depict the histologic features for both normal and malignant laryngeal tissues (Figs. 2–7), which conventionally require multiple paraffin section based staining techniques. Images from the same specimen from the same patient are compared to confirm the feature assignment. It should be noted that because multimodal microscopy was based on optical sectioning of tissue blocks while conventional histological analysis was based on tissue slices, images from these two different processes are from close but not the same tissue locations.

3.1. MPM microscopy of normal laryngeal tissue

The representative images for normal laryngeal epithelium acquired with MPM microscopy [Figs. 2(a)–2(c)] demonstrates normal anatomy comparable to standard paraffin section based histological images [Figs. 2(d)–2(f)]. The composite image from 3PFE, SHG and THG images [Fig. 2(a)] shows the layering structure of typical mucosa including pseudostratified ciliated column epithelium or squamous epithelium, basal lamina, and lamina propria, which can be confirmed by the standard H&E stained image [Fig. 2(d)]. The mucosa mainly consists of ciliated cells that are lined nicely on the surface, with cilia that facilitate the movement of mucus across the airway tract [triangles in Figs. 2(a) and 2(d)]. There is an inflammatory infiltrate in the loose connective tissue beneath the basal lamina [Figs. 2(a) and 2(d)]. The separate modal images from SHG and 3PEF are shown in Figs. 2(b) and 2(c), respectively. Figure 2(b) is the SHG image with signals originating exclusively from collagen fibers due to their non-centrosymmetric molecular structure [30]. The basement membrane is clearly visualized as a thin and continuous fibrous band beneath the mucosa as pointed out by the blue arrow in Fig. 2(b). The lamina propria is mainly made up collagen fibers that form the basic framework of the stroma. These collagen related features are more difficult to discern in H&E images, and normally require Masson staining to visualize [Fig. 2(e)]. Figure 2(c) is the 3PF image providing the cell morphology. The normal cell nuclei without intra-nucleus structures appear to be black holes with regular nucleus
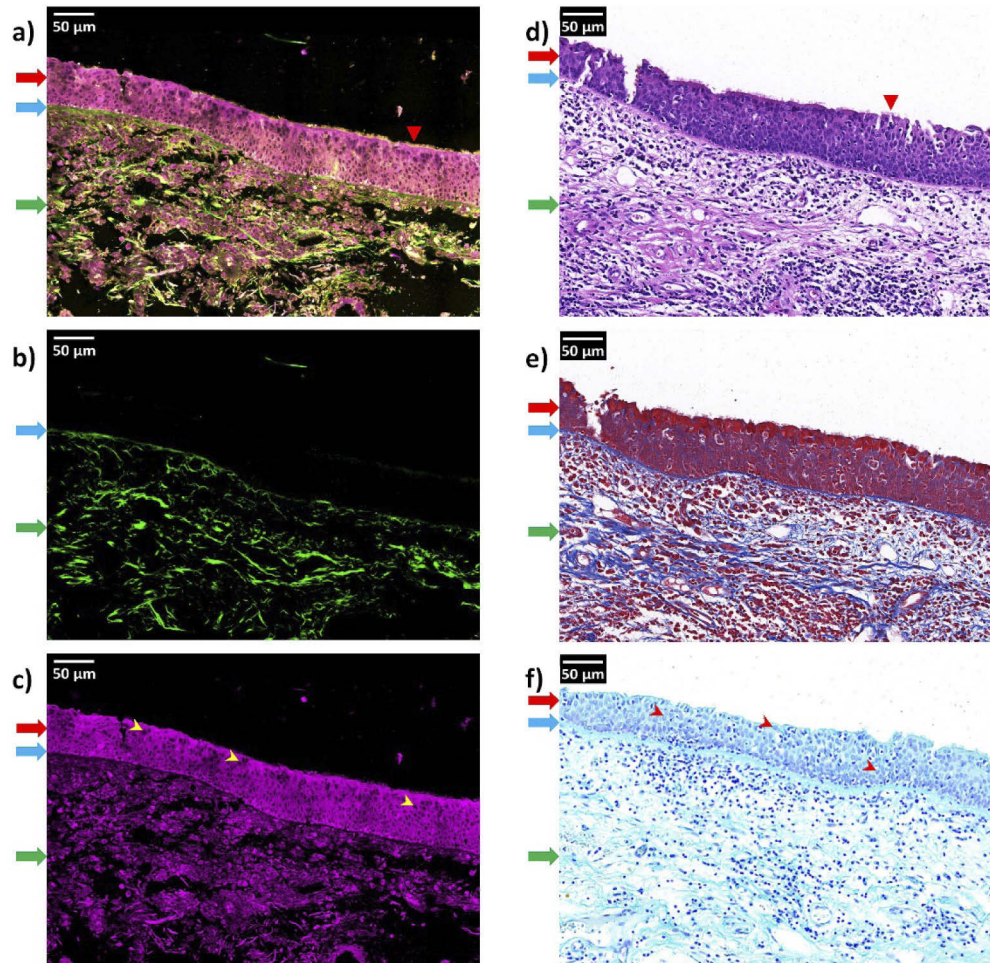
Fig. 2. Representative images from MPM imaging (a-c) and corresponding paraffin section based histological images (d-f) of normal laryngeal epithelium. a) composite image of multiple modals (THG-yellow, SHG-green, 3PFE-magenta); b) SHG image; c) 3PF image; d) H&E stained image; e) Masson stained image (collagen fibers are displayed in blue); f) Feulgen stained image (nuclei are displayed in dark blue). Red arrows: pseudostratified ciliated column epithelium; blue arrows: basal lamina; green arrows: lamina propria; triangles: cilla; arrow heads: cell nuclei.
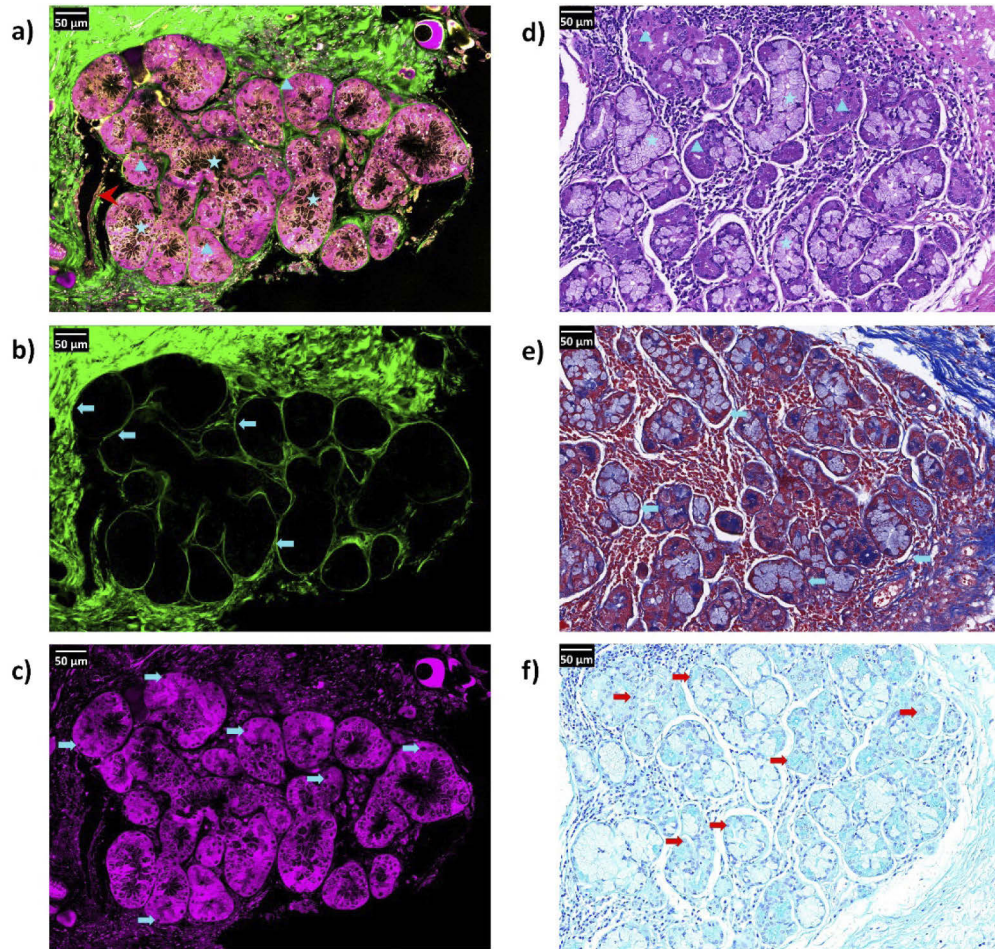
Fig. 3. Representative images from MPM imaging (a-c) and corresponding histological images (d-f) of normal salivary glands. a) composite image of multiple modals (THG-yellow, SHG-green, 3PFE-magenta); b) SHG image; c) 3PF image; d) H&E stained image; e) Masson stained image (collagen fibers are displayed in blue); f) Feulgen stained image (nuclei are displayed in dark blue). Triangles: serous cells; stars: mucous cells; red arrowhead: blood vessel with endothelial cells; left pointing arrows: collagen fibers surrounding individual salivary glands; right pointing arrows: cell nucleus.
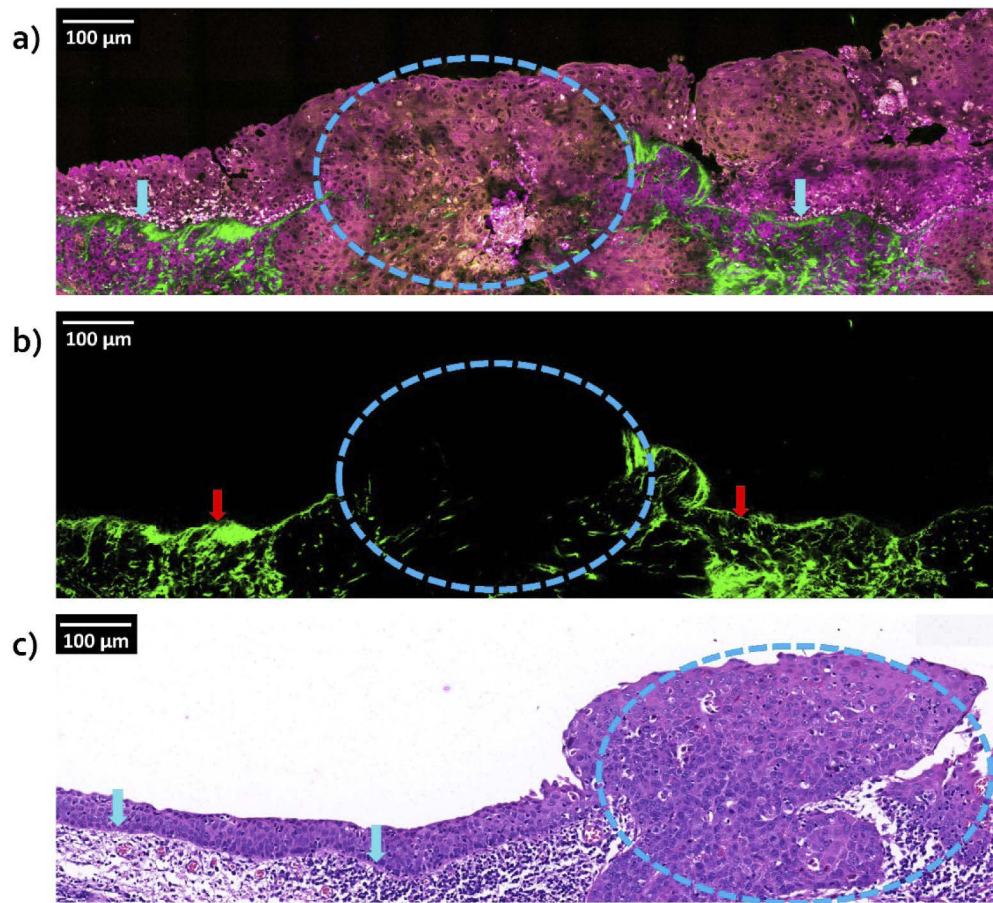
Fig. 4. Representative images from MPM imaging (a, b) and corresponding H&E stained image (c) showing tumor cells invading into lamina propria. a) composite image of multiple modals (THG-yellow, SHG-green, 3PFE-magenta); b) SHG image; c) H&E stained image. Arrows: intact basement membrane; Blue dashed circles: invasion zones.

to cytoplasm ratio [arrowheads in Fig. 2(c)], which are confirmed by the Feulgen stained image [arrowheads in Fig. 2(f)].

There are abundant salivary glands located in the lamina propria of normal laryngeal tissues. The composite multimodal images clearly demonstrate the histological features of typical salivary glands [Fig. 3(a)], which mainly consist of mucus cells (stars) and serous cells (triangles). This is consistent with the standard H&E stained image [Fig. 3(d)]. There is a blood vessel on the left side of the glands, with endothelial cells shown with great details [red arrowhead in Fig. 3(a)]. The SHG image shows the collagen network surrounding individual glands [arrows in Fig. 3(b)], which is difficult to discern from the H&E stained image [Fig. 3(d)]. The 3PEF image displays the cytoplasm and nuclei of cells within normal glands (blue arrows in Fig. 3(c). Identification of these features are confirmed by Masson staining [Fig. 3(e)] and Feulgen staining [Fig. 3(f)], respectively.

3.2. MPM microscopy of malignant laryngeal tissue

Figure 4 shows an example of early stage laryngeal cancer in which the malignant squamous cells invading through the basement membrane into the lamina propria. The multimodal
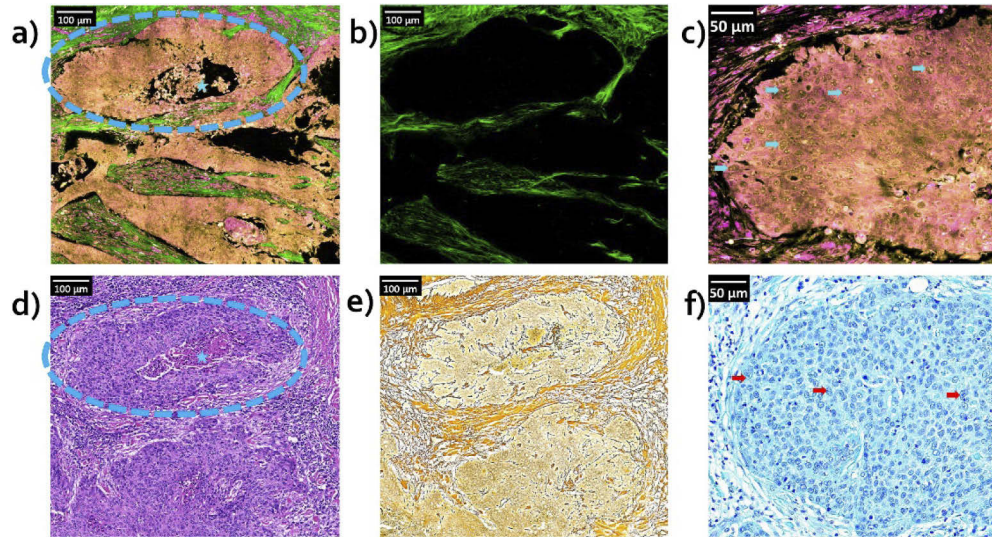
Fig. 5. Representative images from MPM imaging (a-c) and corresponding histological images (d-f) of invasive tumor region. a) composite image of multiple modals (THG-yellow, SHG-green, 3PFE-magenta); b) SHG image; c) zoom in of a malignant region; d) H&E stained image; e) Masson stained image (collagen fibers are displayed in blue); f) Feulgen stained image of a malignant region (nuclei are displayed in dark blue). Stars: tumor necrosis; right pointing arrows: cell nuclei.
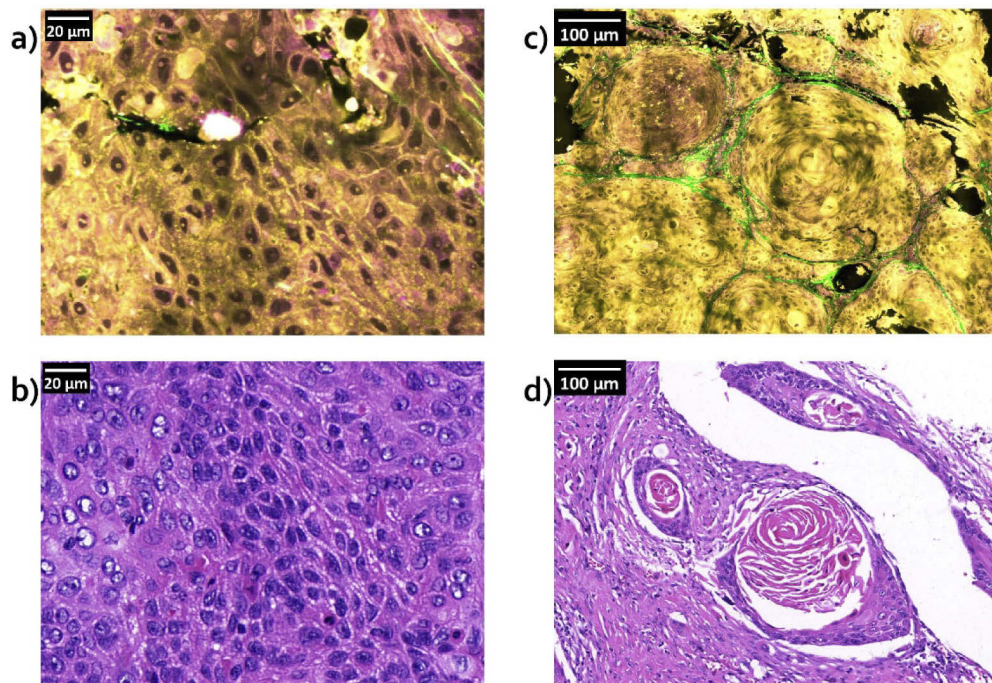

Fig. 6. Representative images from MPM imaging (a, c) and corresponding histological images (b, d) showing characteristic features of squamous cell carcinoma. a) & b) tumor cells with intercellular bridges; c) & d) tumor region showing keratinization.
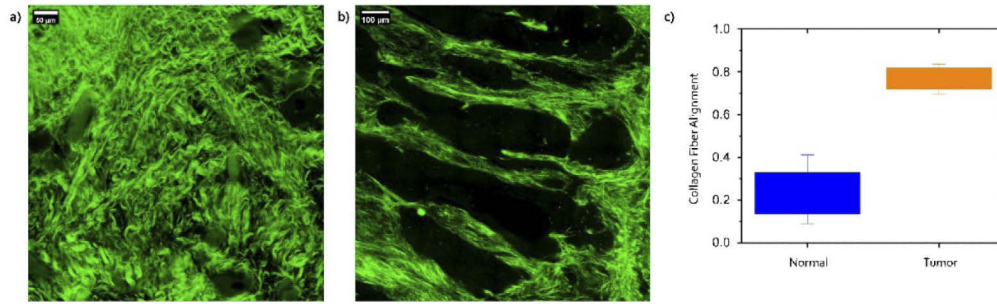
Fig. 7. Representative SHG images from a) normal laryngeal tissue and b) invasive tumor region. c) Comparison of fiber alignment between normal laryngeal tissue and tumors.

microscopy images demonstrate the histological features including the proliferating cells and fibrous structure with high resolution and contrast [Figs. 4(a) and 4(b)], which correlate well with the findings from the H&E stained image [Fig. 4(c)]. For the malignant epithelium, the mucosa is altered with cellular disorganization and thickened with more stratification [Figs. 4(a) and 4(c)]. Epithelial cells become clearly squamous and pleomorphic, losing polarity and columnar tendency, displaying obvious nuclear abnormalities with increased nucleus to cytoplasm ratio. It's worth noting that the degradation of basement membrane at the invasion zone and the increase of the basement membrane thickness beneath the nearby epithelium can be most clearly observed from the SHG image ([Fig. 4(b)].

Two examples of more advanced invasive squamous cell carcinoma are demonstrated in Figs. 5 and 6. With high resolution and contrast, MPM microscopy can identify subtle changes and small features that are critical for determining tumor subtypes and grades [Figs. 5(a)–5(c), Figs. 6(a) and 6(c)], which correlate well with traditional paraffin section-based histology [Figs. 5(d)–5(f), Figs. 6(b) and 6(d)]. In Fig. 5, malignant squamous epithelial cells form irregular large nests with little stromal response [marked regions in Figs. 5(a), 5(d)], disrupting the regular tissue architecture. The altered collagen matrix can be best observed from the SHG image with longer, more aligned fibers [Fig. 5(b)], which is consistent with the Masson stained image of a corresponding paraffin section [blue stain, Fig. 5(e)]. The tumor cells produce THG and 3PEF signals, showing irregular cell morphology and ovoid to spindle shape with indistinct cell borders, and the nuclei are hyperchromatic with multiple prominent nucleoli [arrows in Fig. 5(c and 5(f)]. Central tumor necrosis and limited keratinization are present in this field as well [stars in Fig. 5(a) and 5(c)]. These histological features suggest a "nonkeratinizing with maturation" or poorly differentiated subtype of SCC [31].

In Fig. 6, intercellular bridges [Fig. 6(a)], cell keratinization [Fig. 6(c)], and the formation of keratin pearls [Fig. 6(c)] can be clearly visualized, which are consistent with standard H&E images. The tumor cells are polygonal with distinct cell borders. These cellular and histological features closely resemble the characteristics of normal squamous epithelium, suggesting a "keratinizing" or "well-differentiated" subtype of SCC. The digital nature of these images potentially allows the development of a more quantitative tumor grading system.

3.3. Collagen fiber evaluation

As shown above, collagen fibers can be specifically detected by SHG without staining. Changes of fibrillar morphology can be seen clearly in the case of laryngeal cancer. In normal laryngeal mucosa, collagen fibers appear to be wavy and randomly oriented [Fig. 7(a)]. However, in laryngeal cancer, collagen fibers exhibited clear linearization and irregular alignment [Fig. 7(b)]. In order to investigate whether collagen fiber alignment has the potential to differentiate malignant

tissues from normal tissues, quantitative analysis was performed on the SHG images from 12 normal and 12 malignant ROIs from six patients using CurveAlign software [27–29]. As seen in Fig. 7(c), the collagen fibers in laryngeal cancer are significantly more aligned comparing to their normal counterparts with statistical significance (p<0.001 using paired samples t-test).

4.　Discussion

AF from endogenous fluorophores has been proved to be a powerful tool for direct visualization of tissue morphology, cell metabolism and disease states [6,7,32]. With the experimental settings used in this study, AF mainly comes from the sum of three photon excitation of NADH and FAD from cytoplasm, which displays the morphology of cells and nuclei, and allows the identification of irregular cells in malignant tissues. Previous work using 2PFE has demonstrated the imaging of the epithelium and the lamina propria on normal oral mucosa [18]. Comparing to 2PEF, 3PEF uses longer exciting wavelength which reduces signal from regions out of focus as well as tissue scattering, hence allows better penetration depth [5], providing the potential for enabling *in vivo* imaging of the laryngeal epithelium. Due to the much smaller cross section, 3PEF is even more sensitive to the pulse quality at the sample [26]. Therefore, the precise control of the pulse duration and compensation of the pulse distortion along the light path are critical for achieving efficient imaging using this modality.

It's well known that collagen fiber is a key component of the tumor microenvironment. Remodeling of the collagen architecture occurs in all epithelial malignancies, which substantially influences tumor pathogenesis, progression, metastasis, and response to different therapies. The SHG images of the laryngeal epithelial provide high specificity and resolution for the detection of collagen fiber network including basement membranes, which has been confirmed by a number of earlier studies [10–12]. Collagen fibers are abundant and well organized in lamina propria of normal laryngeal tissues, which is consistent with the findings for oral mucosa [19]. From the images acquired in this study, it seems the thickness of the basement membrane increases in malignant laryngeal epithelia comparing to their normal counterparts [blue arrow in Fig. 2(b) vs. red arrow in Fig. 4(b)]. On the other hand, in laryngeal cancer tissues, the appearance of collagen fibers is significantly transformed, showing bundles with highly aligned fibrils. This could provide a quantitative tool for evaluating the alteration in collagen network during carcinogenesis and tumor progression.

THG in tissue originates from the water-lipid and water-protein interfaces. It's a very useful contrast modality which is complementary to multiphoton fluorescence and SHG imaging, showing the intracellular and extracellular structures such as cellular membranes, nuclear membranes, cell organelles, intracellular lipid droplets, and extracellular vesicles [16]. In the case of laryngeal tissues, THG enables the direct observation of intracellular bridges and keratinization (Fig. 6), which are important for the determination of the squamous origin of the tumor. Similar to multiphoton excitation fluorescence and SHG, THG is only generated in the focal volume which allows for optical sectioning and 3D scanning of tissue samples.

By simultaneously collecting multiple modalities including AF, SHG and THG, label free and slide free imaging of laryngeal tissues is achieved with high resolution and contrast. All microscopic features that were used in standard histological evaluation can be provided by the composite image from multiple modalities, providing the potential for an accurate diagnosis to be made. The histological appearance of the normal laryngeal tissues, including the layered epithelial and salivary glands, is clearly demonstrated and similar to the earlier findings for oral mucosa [18]. The alteration of the epithelium structure and abnormality in cellular morphology allows the identification of malignant laryngeal lesions, which is consistent with the study on hamster check pouch that differentiates normal, precancerous and cancerous tissues [33]. The subtle features such as intracellular bridges, keratinization, and necrosis can be clearly observed and used to determine the subtypes or the grading of the tumor. In addition, the SHG modality images

the collagen network specifically, which is extremely powerful for qualitatively and quantitatively analyzing the extracellular matrix, the desmoplastic reaction in tumor microenvironment, and the alteration in the basement membrane. As indicated in this study, in malignant laryngeal tumors, the basement membrane is degraded at the invasion sites and thickened in nearby mucosa. The collagen fiber appearance and organization in the stroma is altered, and becomes significantly more aligned comparing to those in normal tissue. On the other hand, multiphoton excitation significantly reduces the risk of photo damaging the sample since the excitation occurs only in the immediate focal region, rather than the entire volume light passes as in confocal fluorescence [34].

The number of patients is relatively small in this research, limiting the possibility of more rigorous quantitative analysis. More samples are being collected and will be presented in a future study. In addition, the current work was based on *ex vivo* imaging on fixed sample. We plan to install a FLI microscopy system next to operation room, to further study the *ex vivo* imaging on fresh tissue sample and to investigating *in vivo* optical biopsy. The result will be discussed in future work as well.

5. Conclusion

This work demonstrates the ability of MPM microscopy in generating label-free images of laryngeal tissues with rich information on the tissue and cellular morphology. The image contrast and clarity are comparable, if not superior, to those of standard H&E images, providing the potential for a histologic diagnosis to be made. With this technique, the need for conventional histological sample preparation including embedding, sectioning, and staining can be eliminated which saves time, labor and reduces toxic chemical consumption, allowing fast *ex vivo* and potentially *in vivo* detection of laryngeal lesions to be made at the point of care.

Disclosures. The authors declare no conflicts of interest.

References

1. F. Bray, J. Ferlay, I. Soerjomataram, R. L. Siegel, L. A. Torre, and A. Jemal, "Global cancer statistics 2018: GLOBOCAN estimates of incidence and mortality worldwide for 36 cancers in 185 countries," CA: A Cancer J. for Clin. **68**(6), 394–424 (2018).
2. R. Nocini, G. Molteni, C. Mattiuzzi, and G. Lippi, "Section of Ear Nose and Throat (ENT), Department of Surgical Sciences, Dentistry, Gynecology and Pediatrics, University of Verona, Verona 37134, Italy, Service of Clinical Governance, Provincial Agency for Social and Sanitary Services, Trento 38123, Italy, and Section of Clinical Biochemistry, Department of Neuroscience, Biomedicine and Movement, University of Verona, Verona 37134, Italy, "Updates on larynx cancer epidemiology," Chinese J. Cancer Res. **32**(1), 18–25 (2020).
3. S. Paleologou, "Survival Outcomes in Early Stage Laryngeal Cancer," ANTICANCER RESEARCH 5 (2016).
4. J. Brandstorp-Boesen, R. Sørum Falk, M. Boysen, and K. Brøndbo, "Impact of stage, management and recurrence on survival rates in laryngeal cancer," PLoS One **12**(7), e0179371 (2017).
5. R. M. Martínez-Ojeda, M. D. Pérez-Cárceles, L. C. Ardelean, S. G. Stanciu, and J. M. Bueno, "Multiphoton Microscopy of Oral Tissues: Review," Front. Phys. **8**, 128 (2020).
6. T. T. König, J. Goedeke, and O. J. Muensterer, "Multiphoton microscopy in surgical oncology- a systematic review and guide for clinical translatability," Surg. Oncol. **31**, 119–131 (2019).
7. S. A. Boppart, S. You, L. Li, J. Chen, and H. Tu, "Simultaneous label-free autofluorescence-multiharmonic microscopy and beyond," APL Photonics **4**(10), 100901 (2019).
8. O. Uckermann, R. Galli, G. Mark, M. Meinhardt, E. Koch, G. Schackert, G. Steiner, and M. Kirsch, "Label-free multiphoton imaging allows brain tumor recognition based on texture analysis—a study of 382 tumor patients," Neuro-Oncology Adv. **2**(1), vdaa035 (2020).
9. L. Li, D. Kang, Z. Huang, Z. Zhan, C. Feng, Y. Zhou, H. Tu, S. Zhuo, and J. Chen, "Multimodal multiphoton imaging for label-free monitoring of early gastric cancer," BMC Cancer **19**(1), 295 (2019).
10. Y. Sun, S. You, H. Tu, D. R. Spillman, E. J. Chaney, M. Marjanovic, J. Li, R. Barkalifa, J. Wang, A. M. Higham, N. N. Luckey, K. A. Cradock, Z. George Liu, and S. A. Boppart, "Intraoperative visualization of the tumor microenvironment and quantification of extracellular vesicles by label-free nonlinear imaging," Sci. Adv. **4**(12), eaau5603 (2018).

11. V. Lutz, M. Sattler, S. Gallinat, H. Wenck, R. Poertner, and F. Fischer, "Characterization of fibrillar collagen types using multi-dimensional multiphoton laser scanning microscopy," Int. J. Cosmet Sci. **34**(2), 209–215 (2012).

12. E. B. Brown, "Understanding Collagen Organization in Breast Tumors to Predict and Prevent Metastasis," 221 (2015).

13. S. W. Perry, R. M. Burke, and E. B. Brown, "Two-Photon and Second Harmonic Microscopy in Clinical and Translational Cancer Research," Ann. Biomed. Eng. **40**(2), 277–291 (2012).

14. E. Gavgiotaki, G. Filippidis, H. Markomanolaki, G. Kenanakis, S. Agelaki, V. Georgoulias, and I. Athanassakis, "Distinction between breast cancer cell subtypes using third harmonic generation microscopy," J. Biophotonics **10**(9), 1152–1162 (2017).

15. N. V. Kuzmin, P. Wesseling, P. C. de W. Hamer, D. P. Noske, G. D. Galgano, H. D. Mansvelder, J. C. Baayen, and M. L. Groot, "Third harmonic generation imaging for fast, label-free pathology of human brain tumors," Biomed. Opt. Express **7**(5), 1889 (2016).

16. B. Weigelin, G.-J. Bakker, and P. Friedl, "Third harmonic generation microscopy of cells and tissue organization," J. Cell Sci. **129**(2), 245–255 (2016).

17. G. G. Lee, H.-H. Lin, M.-R. Tsai, S.-Y. Chou, W.-J. Lee, Y.-H. Liao, C.-K. Sun, and C.-F. Chen, "Automatic Cell Segmentation and Nuclear-to-Cytoplasmic Ratio Analysis for Third Harmonic Generated Microscopy Medical Images," IEEE Trans. Biomed. Circuits Syst. **7**(2), 158–168 (2013).

18. S. Zhuo, J. Chen, X. Jiang, S. Xie, R. Chen, N. Cao, Q. Zou, and S. Xiong, "The layered–resolved microstructure and spectroscopy of mouse oral mucosa using multiphoton microscopy," Phys. Med. Biol. **52**(16), 4967–4980 (2007).

19. Y. Wu and J. Y. Qu, "Two-photon autofluorescence spectroscopy and second-harmonic generation of epithelial tissue," Opt. Lett. **30**(22), 3045 (2005).

20. J. Xu, D. Kang, Y. Zeng, S. Zhuo, X. Zhu, L. Jiang, J. Chen, and J. Lin, "Multiphoton microscopy for label-free identification of intramural metastasis in human esophageal squamous cell carcinoma," Biomed. Opt. Express **8**(7), 3360 (2017).

21. S. Mehravar, B. Banerjee, H. Chatrath, B. Amirsolaimani, K. Patel, C. Patel, R. A. Norwood, N. Peyghambarian, and K. Kieu, "Label-free multi-photon imaging of dysplasia in Barrett's esophagus," Biomed. Opt. Express **7**(1), 148 (2016).

22. S. You, H. Tu, E. J. Chaney, Y. Sun, Y. Zhao, A. J. Bower, Y.-Z. Liu, M. Marjanovic, S. Sinha, Y. Pu, and S. A. Boppart, "Intravital imaging by simultaneous label-free autofluorescence-multiharmonic microscopy," Nat. Commun. **9**, 2125 (2018).

23. Z. Chen, W. Guo, D. Kang, S. Wang, L. Zheng, G. Xi, Y. Lian, C. Wang, and J. Chen, "Label-Free Identification of Early Stages of Breast Ductal Carcinoma via Multiphoton Microscopy," Scanning **2020**, 1–8 (2020).

24. J. Yan, X. Zheng, Z. Liu, W. Liu, D. Lin, D. Chen, K. Li, W. Jiang, Z. Li, N. Zuo, G. Chen, J. Lu, J. Chen, G. Li, C. Xu, and S. Zhuo, "Multiphoton imaging provides a superior optical biopsy to that of confocal laser endomicroscopy imaging for colorectal lesions," Endoscopy **51**(02), 174–178 (2019).

25. R. Cicchi, A. Sturiale, G. Nesi, D. Kapsokalyvas, G. Alemanno, F. Tonelli, and F. S. Pavone, "Multiphoton morpho-functional imaging of healthy colon mucosa, adenomatous polyp and adenocarcinoma," Biomed. Opt. Express **4**(7), 1204 (2013).

26. B. Xu, J. M. Gunn, J. M. D. Cruz, V. V. Lozovoy, and M. Dantus, "Quantitative investigation of the multiphoton intrapulse interference phase scan method for simultaneous phase measurement and compensation of femtosecond laser pulses," J. Opt. Soc. Am. B **23**(4), 750–759 (2006).

27. J. S. Bredfeldt, Y. Liu, C. A. Pehlke, M. W. Conklin, J. M. Szulczewski, D. R. Inman, P. J. Keely, R. D. Nowak, T. R. Mackie, and K. W. Eliceiri, "Computational segmentation of collagen fibers from second-harmonic generation images of breast cancer," J. Biomed. Opt. **19**(1), 016007 (2014).

28. Y. Liu, A. Keikhosravi, G. S. Mehta, C. R. Drifka, and K. W. Eliceiri, "Methods for Quantifying Fibrillar Collagen Alignment," Methods Mol. Biol. **1627**, 429–451 (2017).

29. C. R. Drifka, J. Tod, A. G. Loeffler, Y. Liu, G. J. Thomas, K. W. Eliceiri, and W. J. Kao, "Periductal stromal collagen topology of pancreatic ductal adenocarcinoma differs from that of normal and chronic pancreatitis," Mod. Pathol. **28**(11), 1470–1480 (2015).

30. R. M. Williams, W. R. Zipfel, and W. W. Webb, "Interpreting Second-Harmonic Generation Images of Collagen I Fibrils," Biophys. J. **88**(2), 1377–1386 (2005).

31. R. D. Chernock, "Morphologic Features of Conventional Squamous Cell Carcinoma of the Oropharynx: 'Keratinizing' and 'Nonkeratinizing' Histologic Types as the Basis for a Consistent Classification System," Head and Neck Pathol **6**(S1), 41–47 (2012).

32. J. Hou, J. Williams, E. L. Botvinick, E. O. Potma, and B. J. Tromberg, "Visualization of Breast Cancer Metabolism Using Multimodal Nonlinear Optical Microscopy of Cellular Lipids and Redox State," Cancer Res. **78**(10), 2503–2512 (2018).

33. M. C. Skala, J. M. Squirrell, K. M. Vrotsos, J. C. Eickhoff, A. Gendron-Fitzpatrick, K. W. Eliceiri, and N. Ramanujam, "Multiphoton Microscopy of Endogenous Fluorescence Differentiates Normal, Precancerous, and Cancerous Squamous Epithelial Tissues," Cancer Res. **65**(4), 1180–1186 (2005).

34. R. K. P. Benninger and D. W. Piston, "Two-Photon Excitation Microscopy for the Study of Living Cells and Tissues," Curr. Protoc. Cell Biol. **59**, 4.11.1 (2013).